



1 **A global analysis of reconstructed land climate changes during Dansgaard-**
2 **Oeschger events**

3 Mengmeng Liu^{1,2,*}, Iain Colin Prentice¹, Sandy P. Harrison²

4 1: Georgina Mace Centre for the Living Planet, Department of Life Sciences, Imperial College
5 London, Silwood Park Campus, Buckhurst Road, Ascot SL5 7PY, UK

6 2: Department of Geography and Environmental Science, University of Reading, Reading,
7 RG6 6AB, UK

8 * **Corresponding author: m.liu18@imperial.ac.uk**

9

10 **Abstract**

11 Dansgaard–Oeschger (D–O) warming events are comparable in magnitude and rate to the
12 anticipated 21st century warming. As such, they provide a good target for evaluation of the
13 ability of state-of-the-art climate models to simulate rapid climate changes. Despite the wealth
14 of qualitative information about climate changes during the D–O events, there has been no
15 attempt to date to make quantitative reconstructions globally. Here we provide reconstructions
16 of seasonal temperature changes and changes in plant-available moisture across multiple D–O
17 events during Marine Isotope Stage 3 based on available pollen records across the globe. These
18 reconstructions show that the largest changes in temperature occurred in northern extratropics,
19 especially Europe and Eurasia. The change in winter temperature was not significantly different
20 from the change in summer temperature, and thus there is no evidence that the D–O events
21 were characterised by a change in seasonality. Although broadscale features of the temperature
22 changes were consistent across the eight D–O events examined, the spatial patterns of
23 temperature changes vary between events. Globally, changes in moisture were positively
24 correlated with changes in temperature, but the strength and the sign of this relationship vary
25 regionally. These reconstructions can be used to evaluate the spatial patterns of changes in
26 temperature and moisture in the transient simulations of the D–O events planned as part of the
27 Palaeoclimate Modelling Intercomparison Project.



28 **1. Introduction**

29 Dansgaard–Oeschger (D–O) events are characterised in Greenland by a transition from cold
30 Greenland Stadial (GS) to warmer Greenland Interstadial (GI) conditions (Dansgaard et al.,
31 1993). The surface air temperature in Greenland increased by 10–15° C during the warming
32 phases; these warming events occur over an interval of between 50 and 200 years (Huber et
33 al., 2006; Kindler et al., 2014). Thus, the D-O events offer a parallel in terms of speed to
34 projected future warming, although both the baseline state and the mechanism inducing this
35 warming differ from anticipated 21st century climate changes. D-O events could therefore
36 provide an opportunity to determine how well climate models that are used for future
37 projections can simulate rapid climate changes (Malmierca-Vallet et al., 2023).

38 D-O events are registered globally (Voelker, 2002; Sánchez Goñi and Harrison, 2010; Harrison
39 and Sánchez Goñi, 2010; Sánchez Goñi et al., 2017; Adolphi et al., 2019; Corrick et al., 2020).
40 Shifts in vegetation types between GI and GS states have been interpreted as primarily a
41 temperature signal in the extratropics and a moisture signal in the tropics (Harrison and
42 Sánchez Goñi, 2010). Speleothem records provide a good time-control on the synchronicity of
43 climate changes globally with the D-O events registered in Greenland (Adolphi et al., 2019;
44 Corrick et al., 2020), but the driver of this signal can either be temperature or precipitation
45 depending on the region. There are quantitative climate reconstructions based on pollen records
46 from La Grande Pile (Guiot et al., 1993), Lago Grande di Monticchio (Huntley et al., 1999),
47 Padul (Camuera et al., 2022), El Cañizar de Villarquemado (Wei et al., 2021; Camuera et al.,
48 2022) and Lake Ohrid (Sinopoli et al., 2019), diatom assemblages at Les Echets, France
49 (Ampel et al., 2010), bacterial membrane lipid records from the Eifel region (Zander et al.,
50 2023), isotopic measurements of earthworm calcite from the Rhine Valley (Prud'homme et al.,
51 2022) and clumped isotope measurements on snails in Hungary (Újvári et al., 2021). Aside
52 from the lack of comparable quantitative estimates from outside Europe, differences in the
53 methodology employed and in the specific climate variables reconstructed in each of these
54 studies limits their usefulness for model evaluation. In particular, given that there is still
55 uncertainty as to whether the D-O cycles are characterised by changes in seasonality such that
56 warming events are primarily driven by changes in winter (Flückiger et al., 2008; Zander et al.,
57 2023), in the regional strength of the warming (Harrison and Sánchez Goñi, 2010) and how
58 warming relates to changes in moisture (Wei et al., 2021), there is a need for more systematic
59 reconstruction of seasonal climate changes.



60 In the paper, we provide reconstructions of seasonal temperature changes and changes in plant-
61 available moisture across multiple D-O events during Marine Isotope Stage 3 based on
62 available pollen records globally. We employ a standard methodology to construct age models
63 for these records, as well as a standard regression-based approach to make the reconstructions.
64 We analyse the regional patterns to identify key targets for model evaluation.

65 **2. Methods**

66 **2.1. Data sources**

67 Modern pollen data were obtained from version 2 of the SPECIAL Modern Pollen Data Set
68 (SMPDSv2: Villegas-Diaz and Harrison, 2022). This global data set contains 24649 modern
69 pollen records from 17827 sites. The dataset contains relative abundance records for 4816
70 pollen taxa, created after removing taxa that are not climatically diagnostic (e.g. obligate
71 aquatics, carnivorous species, cultivated plants). The data set provides several levels of
72 taxonomic aggregation; here we use the most aggregated level, where woody species were
73 generally combined at genus level and herbaceous species at sub-family or family level unless
74 they were palynologically distinctive, occupied distinctive ecological niches and were
75 sufficiently geographically widespread. This "amalgamated" data set contains relative
76 abundance information for 1338 taxa. These samples were aggregated by longitude, latitude
77 and elevation in order to remove duplicates. Counts for *Quercus*, *Quercus* (deciduous) and
78 *Quercus* (evergreen) were combined because of inconsistent differentiation of *Quercus* pollen
79 in different regional records. Taxa with <10 occurrences were removed to avoid the problem
80 of rarity (Liu et al., 2020). After this filtering, the data set contains 17547 sites (Figure 1) with
81 591 taxa.

82 The SMPDSv2 also provides climatic information at each pollen site, specifically the mean
83 temperature of the coldest month (MTCO), mean temperature of the warmest month (MTWA),
84 and a moisture index (α) calculated as the ratio of actual evapotranspiration to equilibrium
85 evapotranspiration. These bioclimate variables reflect mechanistically distinct controls on
86 plant growth.

87 The fossil pollen data were obtained from the Abrupt Climate Changes and Environmental
88 Responses (ACER) database (Sánchez Goñi et al., 2017), which includes 93 records from the
89 last glacial period (73-15 ka) with sufficient resolution and dating control to detect sub-



90 millennial scale variability. Here we focus on the 73 records covering most of Marine Isotope
91 Stage 3 (50-30 ka); 54 of these records are from terrestrial sites and 19 from continental-shelf
92 marine sites (Figure 1; Table 1). The fossil data were taxonomically harmonised to be
93 consistent with the SMPDSv2.

94 **2.2. Climate reconstruction method**

95 We used tolerance-weighted Weighted Averaging Partial Least Squares (*fxTWA*-PLS; Liu et
96 al., 2020; Liu et al., 2023) regression to model the relationships between taxon abundances and
97 individual climate variables in the SMPDSv2 modern training dataset and then applied these
98 relationships to reconstruct past climate using the fossil assemblages from the ACER database
99 (Figure 2). *fxTWA*-PLS reduces the tendency of regression methods to compress
100 reconstructions towards the centre of the sampled climate range by applying a sampling
101 frequency correction to reduce the influence of uneven sampling of climate space and
102 weighting the contribution of individual taxa according to their climate tolerances (Liu et al.,
103 2020). Version 2 of *fxTWA*-PLS (*fxTWA*-PLS2, Liu et al., 2023) uses P-splines smoothing to
104 derive the frequency correction and applies this correction both in estimating the climate
105 optima and tolerances, and in the regression itself, producing a further improvement in model
106 performance compared to version 1 (Liu et al., 2020).

107 We evaluated the *fxTWA*-PLS models by comparing the reconstructions with observations
108 using leave-out cross-validation, where one site at a time was randomly selected as a test site
109 and geographically and climatically similar sites were removed from the training set to prevent
110 redundancy in the climate information from inflating the cross-validation goodness of fit. We
111 selected the last significant number of components (p -value ≤ 0.01) and assessed model
112 performance using the root mean square error of prediction (RMSEP). Compression was
113 assessed using linear regression and local compression was assessed by loess regression
114 (*locfit*). Reconstructions of MTCO, MTWA and α were made for every sample in each fossil
115 record. Sample specific errors were estimated via bootstrapping, as described in Liu et al.
116 (2020). We corrected for the effect of changes in atmospheric CO₂ on plant water-use
117 efficiency, and hence the reconstructions of α (Figure S1), following Prentice et al. (2022).
118 Appropriate values of CO₂ were taken from the WAIS Divide ice core record (Bauska et al.,
119 2021).



120 **2.3. Age modelling**

121 Although the ACER database provides age models for each pollen record, the resolution of the
122 individual records is variable (mean resolution 474 years) and these models are often
123 imperfectly aligned with the dating of D-O events as recorded in the Greenland ice core. To
124 create a better alignment, we used dynamic time warping (DTW: Belman and Kalaba, 1959;
125 Burstyn et al., 2021) to adjust the age scale for each individual record (Figure 2). Dynamic
126 time warping optimises the similarity between two sequences by stretching or compressing one
127 sequence in the time dimension to match the other. Here, we use simulated mean annual
128 temperature from a transient simulation of the interval 50-30 ka made with the LOVECLIM
129 model (Menviel et al., 2014) as the reference sequence. We used the mid-point between the
130 start dates of each D-O event (Wolff et al., 2010; converted into AICC2012 timescale) to sub-
131 divide each record into discrete intervals. For each site in each interval, we modify the time
132 scale of the reconstructed mean annual temperature series in each ACER record to match the
133 reference, after having normalised both sequences to remove the influence of differences in
134 absolute values and the amplitude of changes. To remove the influence of the variable temporal
135 resolution of the pollen records we interpolated the reconstructions from individual samples to
136 provide estimates at regular intervals (25 years) through each record. The adjusted age model
137 for each site was then applied to the reconstructions of MTCO, MTWA, and α for that site.

138 **2.4. Assessment of changes during D-O events**

139 To estimate the magnitude of climate changes over the D-O events, we used a third-order
140 polynomial to fit the reconstructions during the interval from 300 years before to 600 years
141 after the official start date of each event (Wolff et al., 2010; converted into AICC2012
142 timescale) to obtain the sign of changes (increase or decrease). We used the ages corresponding
143 to the minimum and maximum in the fitted polynomial ($t_{\min \text{ polynomial}}$, $t_{\max \text{ polynomial}}$) but, since
144 the smoothed polynomial may underestimate the amplitude of change, we used the
145 reconstructed minimum or maximum value within the period $t_{\min \text{ polynomial}} \pm 100$ years or t_{\max}
146 $\text{polynomial} \pm 100$ years respectively.

147 In cases where no change was registered for all of the three climate variables, we assume that
148 the event was not registered at the site. As a measure of the accuracy of the DTW method to
149 identify D-O events, we compared the number of identified events with the number of D-O
150 events that occurred during the time covered by each record (Table 1). To assess whether events



151 were missed in a particular record due to low sampling resolution, we examined the number of
152 samples present in the 900-year interval covering the sampled D-O (i.e. 300 years before to
153 600 years after the official start date of each event), where low resolution was defined as ≤ 3
154 samples in this 900-year interval. Reconstructions covering intervals where a signal was not
155 identified were not used in subsequent analyses.

156 3. Results

157 $f\lambda$ TWA-PLS reproduces the modern climate reasonably well (Table 2). The performance is
158 best for MTCO (R^2 0.75, RMSEP 6.51, slope 0.85) but is also good for MTWA (R^2 0.59,
159 RMSEP 3.68, slope 0.71) and α (R^2 0.65, RMSEP 0.18, slope 0.71). Assessment of the variance
160 inflation factor scores shows that there is no problem of multicollinearity so that it is possible
161 to reconstruct all three climate variables independently (Liu et al., 2023).

162 The use of dynamic time-warping made it possible to identify D-O events robustly (Table 1).
163 Across the 73 sites, we identified 204 out of the 210 individual D-O events that occurred during
164 the intervals covered by the records. In the majority of cases where a D-O event should have
165 been registered but could not be identified in an individual record (5 out of 6 cases), the
166 resolution of that part of the record was extremely poor (≤ 3 samples in the 900-year interval
167 starting 300 years before to 600 years after the official start date of the event).

168 Changes in both MTCO and MTWA were generally largest in the extratropics and were more
169 muted in the tropics (Figure 3). The change in MTCO was larger, but not significantly larger,
170 in the northern extratropics when considered across all D-O events and sites; the change in
171 MTCO was smaller, but not significantly smaller, in the southern extratropics; the changes in
172 MTCO are not correlated with the changes in MTWA in the tropics (Table 3). There is a
173 significant positive relationship between the change in α and the change in MTWA in all
174 regions (Figure 4; Table 4).

175 The spatial patterns of changes in MTCO and MTWA show consistent features across multiple
176 D-O events (Figure 5), most noticeably that the largest warming occurs in the extratropics of
177 Europe and Eurasia, while western North America and the southern extratropics are
178 characterised by cooling. The anti-phasing between the northern and southern extratropics is
179 consistent across D-O events. Nevertheless, both the magnitude of the changes and the spatial
180 patterns vary between the D-O events (Figure S2; Figure S3). Changes in α broadly follow the



181 changes in temperature, with increased α in regions characterised by warming (Figure 5) but
182 show more variability both spatially and between D-O events (Figure S4). This is particularly
183 true for Europe, which is characterised by a mixed signal of drying and wetting.

184 **4. Discussion and Conclusions**

185 We have presented a first attempt to map the spatial patterns of quantitative changes in seasonal
186 temperature and plant-available moisture during D-O events globally, using a consistent
187 methodology and a single data source. These analyses show that there is an anti-phasing
188 between changes in the northern extratropics and the southern extratropics, with warming in
189 the north and cooling in the south. The largest and most consistent warming during D-O events
190 occurs in Europe and Eurasia. There is no indication of a significant difference in the
191 temperature change during winter and summer, and thus no indication of a large shift in
192 seasonality as inferred from some site-based reconstructions (e.g. Zander et al., 2023).
193 Globally, there is a positive relationship between the change in temperature and plant available
194 moisture, as indicated by α . This is consistent with more qualitative interpretation of palaeo-
195 records from specific regions, where many regions are characterised by both warming and
196 wetting (e.g. western Europe: Sánchez Goñi et al., 2008; Fletcher et al., 2010; eastern Europe:
197 Fleitmann et al., 2009; Stockehecke et al., 2016; central Siberia: Grygar et al., 2006; the Great
198 Basin USA: Denniston et al., 2007; Jiménez-Moreno et al., 2010). However, according to our
199 reconstructions, the nature of this relationship varies between regions: there are some regions
200 that are characterised by warming and wetting, others are characterised by warming and drying.
201 Previous studies have also indicated drier conditions during D-O events, particularly in parts
202 of the USA such as the Pacific Northwest (Grigg and Whitlock, 2002) and Florida (Grimm et
203 al., 2006; Jiménez-Moreno et al., 2010) Although there is some consistency in the broadscale
204 patterns of changes across D-O events, the magnitude of the changes as well as the spatial
205 patterning varies between events.

206 These reconstructions can be used as targets for model evaluation, specifically the two transient
207 D-O experiments planned for the next phase of the Palaeoclimate Modelling Intercomparison
208 (see Malmierca-Vallet et al., 2023 for the experimental protocol). The first of these experiments
209 is a baseline simulation starting at 34 ka, a time with low obliquity, moderate MIS3 greenhouse
210 gas values, and an intermediate ice sheet configuration, which appears to be most conducive to
211 generating D–O-like behaviour in climate models. The second experiment involves the
212 addition of freshwater, to examine whether this is necessary to precondition a state conducive



213 to generating D–O events. The observed anti-phasing in temperature changes between the
214 northern and southern hemispheres is a general feature of climate model experiments.
215 However, most models show larger warming in winter than in summer in the northern
216 hemisphere (e.g. Flückiger et al., 2008; Van Meersbeeck et al., 2011; Izumi et al., 2023), which
217 is not consistent with our reconstructions. Models generally show an intensification of the
218 northern hemisphere monsoons during D-O events (e.g. Menviel et al., 2020; Izumi et al., 2023),
219 but there is less consistency about changes in plant-available moisture in the extratropics. Our
220 reconstructions of α suggest an intensification of the monsoon over northern South America
221 but there are no records from other northern hemisphere monsoon regions. However, the
222 records do provide an opportunity to evaluate moisture changes over the extratropics.

223 Identifying D-O events in pollen records is often problematic, particularly in regions where
224 warming (especially if accompanied by dryer conditions) leads to a reduction (or an hiatus) in
225 sedimentation as reflected in the variable resolution of the available pollen records (e.g.
226 Sinopoli et al., 2019; Wei et al., 2021; Camuera et al., 2022; Pini et al., 2022). Interpolation of
227 the reconstructed climate between more sparsely spaced samples goes some way to improving
228 the identification of potential D-O events using dynamic time warping, as does the use of
229 shorter periods (Alshehri et al., 2019). However, it is likely that some of the variability in the
230 reconstructed changes between different D-O events reflects imperfect identification of
231 specific events because of the comparatively modest resolution of the records. Several new
232 high-resolution records covering MIS3 have become available since the compilation of the
233 ACER database (e.g. Wei et al., 2021; Camuera et al., 2022; Pini et al., 2022) and including
234 these newer records could help to improve the reliability of the global reconstructions presented
235 here. Nevertheless, this first compilation of quantitative climate reconstructions through
236 multiple D-O events during MIS3 provides an opportunity for evaluation of the transient D-O
237 simulations planned as part of the next phase of the Palaeoclimate Modelling Intercomparison
238 Project (Malmierca-Vallet et al., 2023).

239

240 **Data and code availability.** All the data used are public access and cited here. The code used
241 to generate the reconstructions and figures is available at [https://github.com/ml4418/DO-](https://github.com/ml4418/DO-climate-reconstruction-paper.git)
242 [climate-reconstruction-paper.git](https://github.com/ml4418/DO-climate-reconstruction-paper.git)



243 **Author contributions.** ML, SPH and ICP designed the study. ML made the reconstructions
244 and produced the figures and tables. ML and SPH carried out the analyses. SPH wrote the first
245 draft of the paper and all authors contributed to the final draft.

246 **Competing Interests.** The authors declare not competing interests.

247 **Acknowledgements.** ML acknowledges support from Imperial College through the Lee
248 Family Scholarship. ICP acknowledges support from the ERC under the European Union
249 Horizon 2020 research and innovation programme (grant agreement no.: 787203 REALM).
250 SPH acknowledges fruitful discussions with colleagues from the D-O community working
251 group.

252

253 **References**

254 Adolphi, F., Bronk Ramsey, C., Erhardt, T., Edwards, R. L., Cheng, H., Turney, C. S. M.,
255 Cooper, A., Svensson, A., Rasmussen, S. O., Fischer, H., and Muscheler, R.:
256 Connecting the Greenland ice-core and U / Th timescales via cosmogenic
257 radionuclides: testing the synchronicity of Dansgaard–Oeschger events, *Clim. Past*, 14,
258 1755–1781, <https://doi.org/10.5194/cp-14-1755-2018>, 2018.

259 Alshehri, M., Coenen, F., and Dures, K.: Effective sub-sequence-based dynamic time warping.
260 In: Bramer, M., Petridis, M. (eds) *Artificial Intelligence XXXVI. SGAI 2019. Lecture*
261 *Notes in Computer Science*, 11927. Springer, Cham. [https://doi.org/10.1007/978-3-](https://doi.org/10.1007/978-3-030-34885-4_23)
262 [030-34885-4_23](https://doi.org/10.1007/978-3-030-34885-4_23), 2019.

263 Ampel, L., Bigler, C., Wohlfarth, B., Risberg, J., Lotter, A.F., and Veres, D.: Modest summer
264 temperature variability during DO cycles in western Europe, *Quat. Sci. Rev.*, 29, 1322–
265 1327, <https://doi.org/10.1016/j.quascirev.2010.03.002>, 2010.

266 Bauska, T. K., Marcott, S. A. and Brook, E. J.: Abrupt changes in the global carbon cycle
267 during the last glacial period, *Nat. Geosci.*, 14(2), 91–96, doi:10.1038/s41561-020-
268 00680-2, 2021.



- 269 Bellman, R., and Kalaba, R.: On adaptive control processes, *Automatic Control, IRE*
270 *Transactions*, 4, 1–9, http://ieeexplore.ieee.org/xpls/abs_all.jsp?arnumber=1104847,
271 1959.
- 272 Burstyn, Y., Gazit, A., and Omri Dvir, O.: Hierarchical Dynamic Time Warping methodology
273 for aggregating multiple geological time series, *Comp. & Geosci.*, 150, 104704,
274 <https://doi.org/10.1016/j.cageo.2021.104704>, 2021.
- 275 Camuera, J., Ramos-Román, M.J., Jiménez-Moreno, G. *et al.*: Past 200 kyr hydroclimate
276 variability in the western Mediterranean and its connection to the African Humid
277 Periods, *Sci. Rep.*, 12, 9050, <https://doi.org/10.1038/s41598-022-12047-1>, 2022.
- 278 Corrick, E.C., Drysdale, R.N., Hellstrom, J.C., Capron, E., Rasmussen, S.O., Zhang, X.,
279 Fleitmann, D., Couchoud, I., and Wolff, E.: Synchronous timing of abrupt climate
280 changes during the last glacial period, *Science*, 369, 963–969,
281 <https://doi.org/10.1126/science.aay5538>, 2020.
- 282 Dansgaard, W., Johnsen, S.J., Clausen, H.B., Dahl-Jensen, D., Gundestrup, N.S., Hammer,
283 C.U., Hvidberg, C.S., Steffensen, J.P., Sveinbjörnsdóttir, A.E., Jouzel, J., and Bond,
284 G.: Evidence for general instability of past climate from a 250-kyr ice-core record,
285 *Nature*, 364, 218–220, <https://doi.org/10.1038/364218a0>, 1993.
- 286 Denniston, R.F., Asmerom, Y., Polyak, V., Dorale, J.A., Carpenter, S.J., Trodick, C., Hoye,
287 B., and González, L.A.: Synchronous millennial-scale climatic changes in the Great
288 Basin and the North Atlantic during the last interglacial. *Geology* 35, 619-622, 2007.
- 289 Fleitmann, D., Cheng, H., Badertscher, S., Edwards, R.L., Mudelsee, M., Göktürk, O.M.,
290 Fankhauser, A., Pickering, R., Raible, C.C., Matter, A., Kramers, J., and Tüysüz, O.:
291 Timing and climatic impact of Greenland interstadials recorded in stalagmites from
292 northern Turkey, *Geophys. Res. Lett.*, 36, 2009.
- 293 Fletcher, W.F., Sánchez Goñi, M.F., Allen, J.R.M., Cheddadi, R., Combourieu-Nebout, N.,
294 Huntley, B., Lawson, I., Londeix, L., Magri, D., Margari, V., Müller, U.C., Naughton,
295 F., Novenko, E., Roucoux, K., Tzedakis, P.C.: Millennial-scale variability during the
296 last glacial in vegetation records from Europe, *Quat. Sci. Rev.*, 29, 2839-2864,
297 <https://doi.org/10.1016/j.quascirev.2009.11.015>, 2010.



- 298 Flückiger, J., Knutti, R., White, J.W.C., and Renssen, H.: Modeled seasonality of glacial abrupt
299 climate events, *Clim. Dyn.*, 31, 633–645, <https://doi.org/10.1007/s00382-008-0373-y>,
300 2008.
- 301 Grigg, L.D., and Whitlock, C.: Patterns and causes of millennial-scale climate change in the
302 Pacific Northwest during Marine Isotope Stages 2 and 3, *Quat. Sci. Rev.*, 21, 2067-
303 2083, 2002.
- 304 Grimm, E.C., Watts, W.A., Jacobson, G.L., Hansen, B.C.S., Almquist, H., and Dieffenbacher-
305 Krall, A.C.: Evidence for warm wet Heinrich events in Florida, *Quat. Sci. Rev.*, 25,
306 2197-2211, 2006.
- 307 Grygar, T., Kadlec, J., Pruner, P., Swann, G., Bezdicka, P., Hradil, D., Lang, K., Novotna, K.,
308 and Oberhänsli, H.: Paleoenvironmental record in Lake Baikal sediments:
309 environmental changes in the last 160 ky, *Palaeogeogr. Palaeoclimatol. Palaeoecol.*,
310 237, 240-254, 2006.
- 311 Guiot, J., de Beaulieu, J. L., Cheddadi, R., David, F., Ponel, P., and Reille, M.: The climate in
312 Western Europe during the last Glacial/Interglacial cycle derived from pollen and insect
313 remains, *Palaeogeogr., Palaeoclimatol., Palaeoecol.*, 103, 73–93,
314 [https://doi.org/10.1016/0031-0182\(93\)90053-L](https://doi.org/10.1016/0031-0182(93)90053-L), 1993.
- 315 Jiménez-Moreno, G., Anderson, R.S., Desprat, S., Grigg, L.D., Grimm, E.C., Heusser, L.E.,
316 Jacobs, B.F., López-Martínez, C., Whitlock, C.L., and Willard, D.A.: Millennial-scale
317 variability during the last glacial in vegetation records from North America, *Quat. Sci.*
318 *Rev.*, 29, 2865-2881, <https://doi.org/10.1016/j.quascirev.2009.12.013>, 2010.
- 319 Harrison, S.P., and Sánchez Goñi, M.F.: Global patterns of vegetation response to millennial-
320 scale variability during the last glacial: A synthesis. *Quat. Sci. Rev.*, 29, 2957-2980,
321 2010.
- 322 Huber, C., Leuenberger, M., Spahni, R., Flückiger, J., Schwander, J., Stocker, T.F., Johnsen,
323 S., Landais, A., and Jouzel, J.: Isotope calibrated Greenland temperature record over
324 Marine Iso- tope Stage 3 and its relation to CH₄, *Earth Planet. Sci. Lett.*, 243, 504–519,
325 2006.



- 326 Huntley, B., Watts, W.A., Allen, J.R.M., Zolitschka, B.: Palaeoclimate, chronology and
327 vegetation history of the Weichselian Lateglacial: comparative analysis of data from
328 three cores at Lago Grande di Monticchio, southern Italy, *Quat. Sci. Rev.*, 18: 945-960,
329 [https://doi.org/10.1016/S0277-3791\(99\)00007-4](https://doi.org/10.1016/S0277-3791(99)00007-4), 1999.
- 330 Kindler, P., Guillevic, M., Baumgartner, M., Schwander, J., Landais, A., and Leuenberger, M.:
331 Temperature reconstruction from 10 to 120 kyr b2k from the NGRIP ice core, *Clim.
332 Past*, 10, 887–902, <https://doi.org/10.5194/cp-10-887-2014>, 2014.
- 333 Liu, M., Prentice, I.C., ter Braak, C.J.F. and Harrison, S.P.: An improved statistical approach
334 for reconstructing past climates from biotic assemblages, *Proc. Royal Soc., Math. A*,
335 476, 20200346, 20200346, <https://doi.org/10.1098/rspa.2020.0346>, 2020.
- 336 Liu, M., Shen, Y., González-Sampériz, P., Gil-Romera, G., ter Braak, C.J.F. Prentice, I.C., and
337 Harrison, S.P.: Holocene climates of the Iberian Peninsula, *Clim. Past* 19, 803-834,
338 <https://doi.org/10.5194/cp-19-803-2023>, 2023.
- 339 Malmierca-Vallet, I., Sime, L.C., and the D–O community members: Dansgaard–Oeschger
340 events in climate models: review and baseline Marine Isotope Stage 3 (MIS3) protocol,
341 *Clim. Past*, 19, 915–942, <https://doi.org/10.5194/cp-19-915-2023>, 2023.
- 342 Menviel, L., Timmermann, A., Friedrich, T., and England, M. H.: Hindcasting the continuum
343 of Dansgaard–Oeschger variability: mechanisms, patterns and timing, *Clim. Past* 10,
344 63–77, 2014.
- 345 Menviel, L.C., Skinner, L.C., Tarasov, L., and Tzedakis, P.C.: An ice–climate oscillatory
346 framework for Dansgaard–Oeschger cycles, *Nat. Rev. Earth Environ.*, 1, 677–693,
347 <https://doi.org/10.1038/s43017-020-00106-y>, 2020.
- 348 Pini, R., Furlanetto, G., Vallé, F., Badino, F., Wick, L., Anselmetti, F.S., Bertuletti, P., Fusi, N.,
349 Morlock, M.A., Delmonte, B., Harrison, S.P., Maggi, V., Ravazzi, C.: Linking North
350 Atlantic and Alpine Last Glacial Maximum climates via a high-resolution pollen-based
351 subarctic forest steppe record, *Quat. Sci. Rev.*, 294, 107759,
352 <https://doi.org/10.1016/j.quascirev.2022.107759>, 2022.



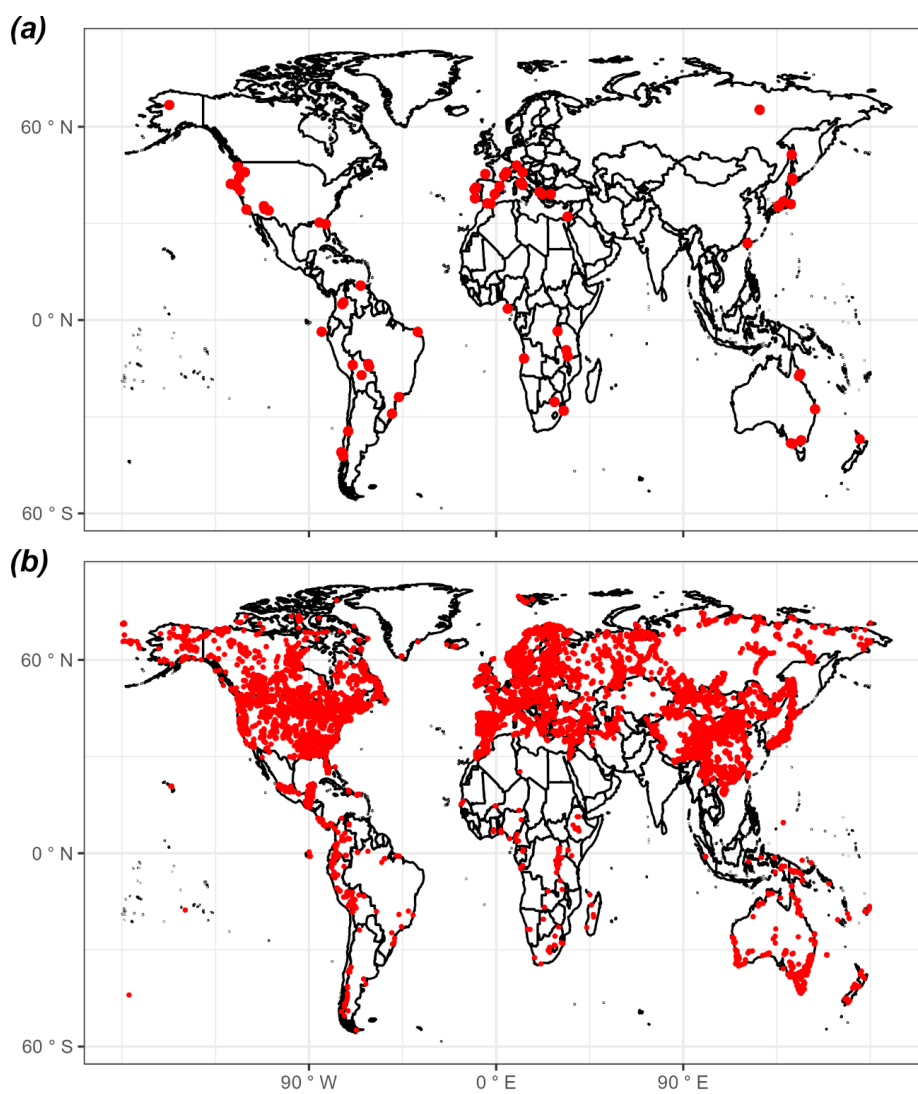
- 353 Prentice, I. C., Villegas-Diaz, R. and Harrison, S. P.: Accounting for atmospheric carbon
354 dioxide variations in pollen-based reconstruction of past hydroclimates, *Glob. Planet.*
355 *Change*, 211, 103790, doi:10.1016/j.gloplacha.2022.103790, 2022.
- 356 Prud'homme, C., Fischer, P., Jöris, O., Gromov, S., Vinnepond, M., Hatté, C., Vonhof, H.,
357 Moine, O., Vött, A., and Fitzsimmons, K. E.: Millennial-timescale quantitative
358 estimates of climate dynamics in central Europe from earthworm calcite granules in
359 loess deposits, *Commun. Earth Environ.*, 3, 1–14, [https://doi.org/10.1038/s43247-022-](https://doi.org/10.1038/s43247-022-00595-3)
360 00595-3, 2022.
- 361 Sánchez Goñi, M.F., and Harrison, S.P.: Millennial-scale climate variability and vegetation
362 changes during the Last Glacial: Concepts and terminology, *Quat. Sci. Rev.*, 29, 2823–
363 2827, 2010.
- 364 Sánchez Goñi, M.F., Desprat, S., Daniau, A.-L., Bassinot, F., Polanco-Martínez, J.M., Harrison,
365 S.P., Allen, J.R.P., Anderson, R.S., Behling, H., Bonnefille, R., Burjachs, F., Carrión,
366 J.S., Cheddadi, R., Clark, J.S., Combourieu-Nebout, N., Courtney-Mustaphi, C.,
367 Debusk, G.H., Dupont, L.M., Finch, J., Fletcher, W.J., Giardini, M., González, C.,
368 Gosling, W.D., Grigg, L.D., Grimm, E.C., Hayashi, R., Helmens, K., Heusser, L.E.,
369 Hill, T., Hope, G., Huntley, B., Igarashi, Y., Irino, T., Jacobs, B.F., Jiménez-Moreno, G.,
370 Kawai, S., Kershaw, P., Kumon, F., Lawson, I., Ledru, M.-P., Lézine, A.-M., Liew, P.-
371 M., Magri, D., Marchant, R., Margari, V., Mayle, F., McKenzie, M., Moss, P., Müller,
372 S., Müller, U.C., Naughton, F., Newnham, R.M., Oba, T., Pérez-Obiol, R., Pini, R.,
373 Ravazzi, C., Roucoux, K.H., Rucina, S., Scott, L., Takahara, H., Tzedakis, P.C., Urrego,
374 D.H., Van Geel, B., Valencia, B.G., Vandergoes, M.J., Vincens, A., Whitlock, C.L.,
375 Willard, D. A., and Yamamoto, M.: The ACER pollen and charcoal database: a global
376 resource to document vegetation and fire response to abrupt climate changes of the last
377 glacial period, *Earth Syst. Sci. Data* 9: 679-695, 2017.
- 378 Sinopoli, G., Peyron, O., Masi, A., Holtvoeth, J., Francke, A., Wagner, B., and Sadori, L.:
379 Pollen-based temperature and precipitation changes in the Ohrid Basin (western
380 Balkans) between 160 and 70 ka, *Clim. Past*, 15, 53–71, [https://doi.org/10.5194/cp-15-](https://doi.org/10.5194/cp-15-53-2019)
381 53-2019, 2019.
- 382 Stockhecke, M., Timmermann, A., Kipfer, R., Haug, G.H., Kwiecien, O., Friedrich, T.,
383 Meniel, L., Litt, T., Pickarski, N., and Anselmetti, F.S.: Millennial to orbital-scale



- 384 variations of drought intensity in the Eastern Mediterranean, *Quat. Sci. Rev.*, 133, 77-
385 95, 2016.
- 386 Újvári, G., Bernasconi, S. M., Stevens, T., Kele, S., Páll-Gergely, B., Surányi, G., and Demény,
387 A.: Stadial-Interstadial Temperature and Aridity Variations in East Central Europe
388 Preceding the Last Glacial Maximum, *Paleoceanog. Paleoclim.*, 36, e2020PA004170,
389 <https://doi.org/10.1029/2020PA004170>, 2021.
- 390 Van Meerbeeck, C.J., Renssen, H., Roche, D.M., Wohlfarth, B., Bohncke, S.J.P., Bos, J.A.A.,
391 Engels, S., Helmens, K.F., Sánchez-Goñi, M.F., Svensson, A., and Vandenberghe, J.:
392 The nature of MIS 3 stadial-interstadial transitions in Europe: New insights from
393 model-data comparisons, *Quat. Sci. Rev.*, 30, 3618–3637,
394 <https://doi.org/10.1016/j.quascirev.2011.08.002>, 2011.
- 395 Villegas-Diaz, R., and Harrison, S.P.: The SPECIAL Modern Pollen Data Set for Climate
396 Reconstructions, version 2 (SMPDSv2). University of Reading.
397 Dataset. <https://doi.org/10.17864/1947.000389>, 2022.
- 398 Voelker, A.H.: Global distribution of centennial-scale records for Marine Isotope Stage (MIS)
399 3: a database, *Quat. Sci. Rev.*, 21, 1185–1212, 2002.
- 400 Wei, D., González-Sampériz, P., Gil-Romera, G., Harrison, S.P., and Prentice, I.C.: Seasonal
401 temperature and moisture changes in interior semi-arid Spain from the last interglacial
402 to the Late Holocene, *Quat. Res.*, 101, 143–155, <https://doi.org/10.1017/qua.2020.108>,
403 2021.
- 404 Wolff, E. W., Chappellaz, J., Blunier, T., Rasmussen, S. O. and Svensson, A.: Millennial-scale
405 variability during the last glacial: The ice core record, *Quat. Sci. Rev.*, 29(21), 2828–
406 2838, doi:10.1016/j.quascirev.2009.10.013, 2010.
- 407 Zander, P.D., Böhl, D., Sirocko, F., Auderset, A., Haug, G., and Martínez-García, A.:
408 Reconstruction of warm season temperatures in central Europe during the past 60,000
409 years from lacustrine GDGTs, *EGUsphere* [preprint],
410 <https://doi.org/10.5194/egusphere-2023-1960>, 2023.

412 **Figures and Tables**

413 Figure 1: Map showing the locations of sites (a) from the Abrupt Climate Changes and
414 Environmental Responses (ACER) database (Sánchez Goñi et al., 2017) covering the interval
415 between 50 ka and 30 ka used for the reconstructions and (b) sites in version 2 of the SPECIAL
416 Modern Pollen Data Set (SMPDSv2: Villegas-Diaz and Harrison, 2022) used to derive the
417 transfer functions for these climate reconstructions.

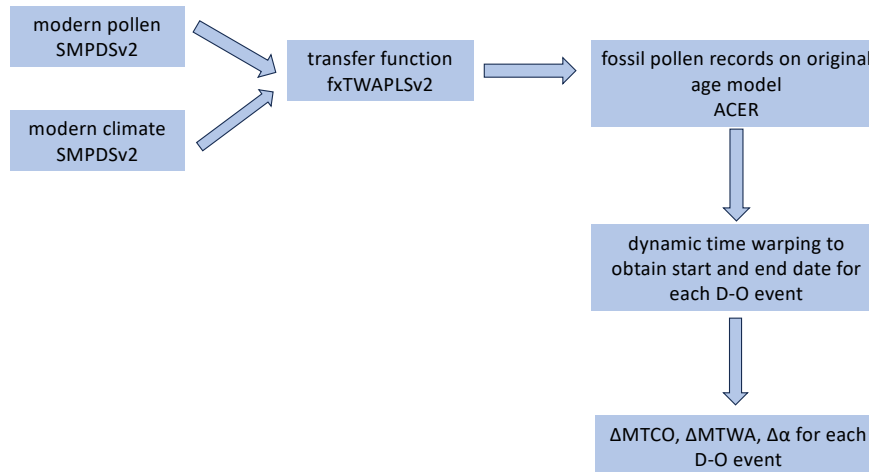


418

419



420 Figure 2: Flow chart showing the reconstruction methodology.



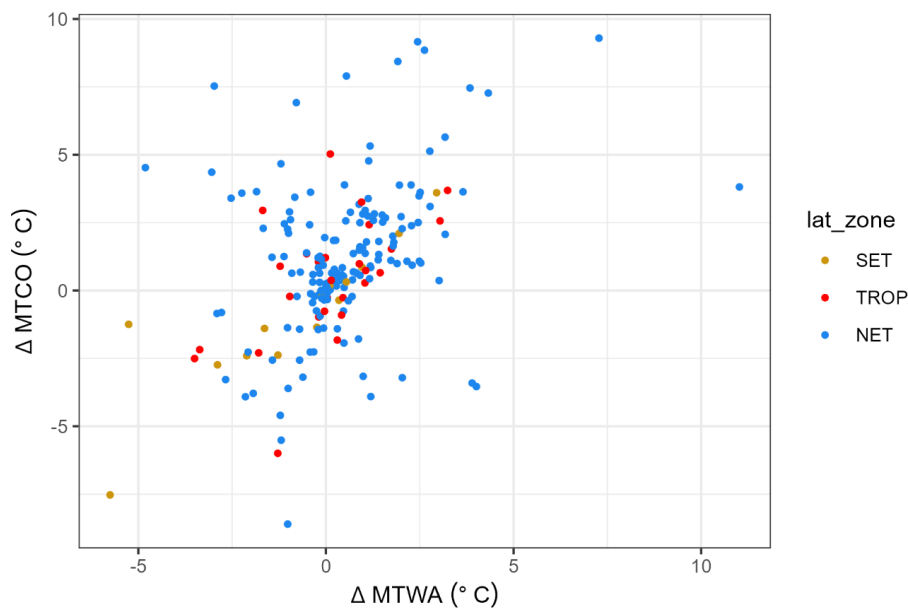
421

422

423

424

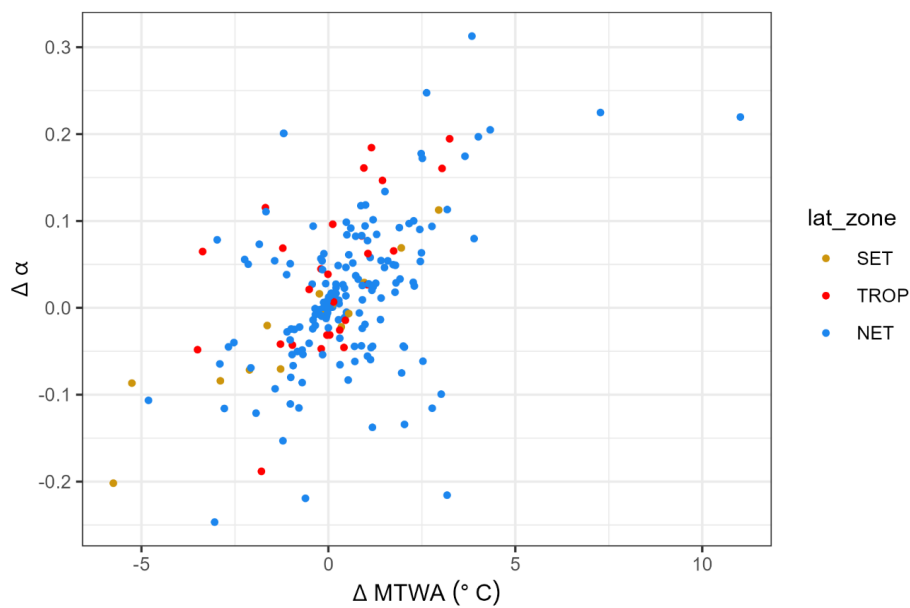
425 Figure 3: Scatter plot of the change in mean temperature of the coldest month (ΔMTCO) versus
426 the change in mean temperature of the warmest month (ΔMTWA) during individual
427 Dansgaard-Oeschger (D-O) events at individual sites. The points are colour-coded to indicate
428 whether the sites are from the northern extratropics (NET, north of 23.5°N), the tropics (TROP,
429 between 23.5°N and 23.5°S) or southern extratropics (SET, south of 23.5°S).



430

431

432 Figure 4: Scatter plot of the change in plant-available moisture ($\Delta\alpha$) versus the change in mean
433 temperature of the warmest month (ΔMTWA) during individual Dansgaard-Oeschger (D-O)
434 events at individual sites. The points are colour-coded to indicate whether the sites are from
435 the northern extratropics (NET, north of 23.5°N), the tropics (TROP, between 23.5°N and
436 23.5°S) or southern extratropics (SET, south of 23.5°S).

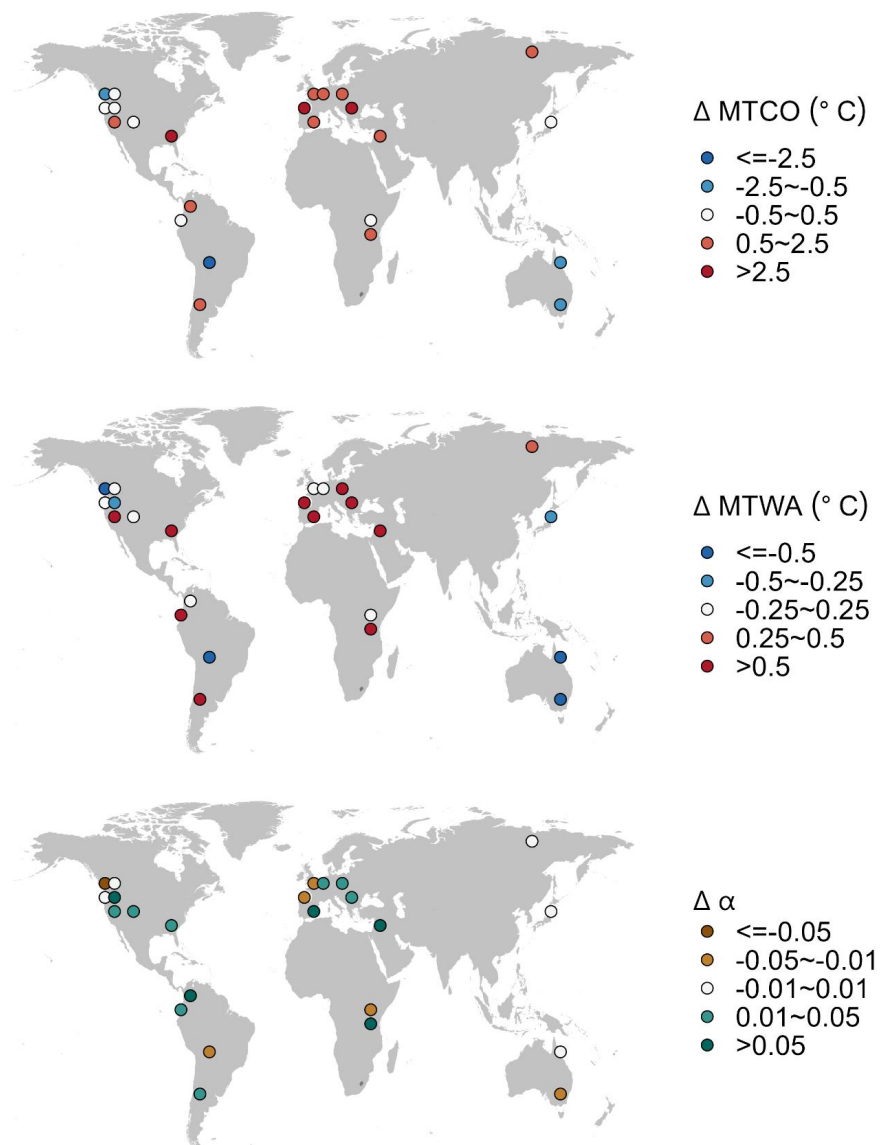


437

438



439 Figure 5: Maps showing the median change of site-based reconstructions for Dansgaard-
440 Oeschger (D-O) events.



441

442



443 Table 1: Details of the 73 sites from the Abrupt Climate Changes and Environmental Responses
 444 (ACER) database (Sánchez Goñi et al., 2017) covering the interval between 50 ka and 30 ka
 445 used for the climate reconstructions. n_{due} is the number of D-O events that should be found
 446 based on the time interval covered by the record. n_{miss} is the number of D-O events that were
 447 not identified. $n_{\text{miss_low_res}}$ is the number of D-O events missed because of low resolution of part
 448 of the record. Six of the D-O events out of the 210 that should have been registered were not
 449 identified, of which 5 are because of low resolution. Reconstructions based on samples where
 450 the D-O signal was not identified were not used in subsequent analyses. Some of the 73 sites
 451 (indicated by / in n_{due} , n_{miss} and $n_{\text{miss_low_res}}$) provide records for parts of the 50-30ka interval but
 452 not for the intervals of the D-O events.

Site name	Latitude	Longitude	Elevation (m)	Site type	n_{due}	n_{miss}	$n_{\text{miss_low_res}}$
Abric Roman	41.53	1.68	350	TERR	/	/	/
Azzano Decimo	45.88	12.72	10	TERR	8	0	0
Caledonia Fen	-37.33	146.73	1280	TERR	/	/	/
Cambara do Sul	-29.05	-50.10	1040	TERR	/	/	/
Camel Lake	30.26	-85.01	20	TERR	3	1	1
Carp Lake	45.91	-120.88	720	TERR	8	0	0
Colnia	-23.87	-46.71	900	TERR	/	/	/
Core Trident 163 31B	-3.61	-83.96	-3210	MARI	1	0	0
Fargher Lake	45.88	-122.58	200	TERR	8	0	0
Framoos	47.98	9.88	662	TERR	/	/	/
Fundo Nueva	-41.28	-73.83	66	TERR	/	/	/
Fuquene	5.45	-73.46	2540	TERR	7	1	1
GeoB3104	-3.67	-37.72	-767	MARI	/	/	/
Hay Lake	34.00	-109.43	2780	TERR	6	1	1
Ioannina	39.75	20.85	470	TERR	8	0	0
Joe Lake	66.77	-157.22	183	TERR	/	/	/
Kalaloch - DIGI	47.61	-124.37	19	TERR	8	0	0



Kamiyoshi Basin (KY01)	35.10	135.59	335	TERR	1	0	0
Kashiru Bog	-3.47	29.57	2240	TERR	8	1	1
Kenbuchi Basin	44.05	142.38	135	TERR	/	/	/
Khoe	51.34	142.14	15	TERR	/	/	/
Kohuora	-36.95	174.87	5	TERR	/	/	/
Kurota Lowland	35.52	135.88	20	TERR	/	/	/
KW31	3.52	5.57	-1181	MARI	/	/	/
La Laguna	4.92	-74.03	2900	TERR	2	0	0
Lac du Bouchet - DIGI	44.83	3.82	1200	TERR	/	/	/
Lagaccione	42.57	11.80	355	TERR	/	/	/
Laguna Bella Vista	-13.62	-61.55	600	TERR	/	/	/
Laguna Chaplin	-14.47	-61.07	600	TERR	/	/	/
Lake Billyakh	65.28	126.78	340	TERR	8	0	0
Lake Biwa (BIW95-4)	35.25	136.05	84	TERR	/	/	/
Lake Consuelo (CON1)	-13.95	-68.99	1360	TERR	/	/	/
Lake Malawi	-11.22	34.42	470	TERR	/	/	/
Lake Masoko	-9.33	33.75	840	TERR	2	0	0
Lake Nojiri	36.83	138.22	657	TERR	8	0	0
Lake Tulane	29.83	-81.95	36	TERR	/	/	/
Lake Wangoom LW87 core	-38.35	142.60	100	TERR	8	0	0
Lake Xinias	39.05	22.27	500	TERR	/	/	/
Les Echets G - DIGI	45.90	4.93	267	TERR	8	0	0
Little Lake	44.16	-123.58	217	TERR	5	0	0
Lynchs Crater	-17.37	145.70	760	TERR	8	0	0
MD01-2421	36.02	141.77	-2224	MARI	/	/	/
MD03-2622 Cariaco Basin	10.71	-65.17	-877	MARI	/	/	/
MD04-2845	45.35	-5.22	-4100	MARI	8	0	0



MD84-629	32.07	34.35	-745	MARI	8	0	0
MD95-2039	40.58	-10.35	-3381	MARI	8	0	0
MD95-2042	37.80	-10.17	-3148	MARI	/	/	/
MD95-2043	36.14	-2.62	-1841	MARI	8	0	0
MD99-2331	41.15	-9.68	-2110	MARI	8	0	0
Megali Limni	39.10	26.32	323	TERR	/	/	/
Mfabeni Peatland	-28.15	32.52	11	TERR	/	/	/
Nakafurano	43.37	142.43	173	TERR	/	/	/
Native Companion Lagoon	-27.68	153.41	20	TERR	/	/	/
Navarrs	39.10	-0.68	225	TERR	3	1	0
ODP 1233 C	-41.00	-74.45	-838	MARI	/	/	/
ODP 820	-16.63	146.30	-280	MARI	/	/	/
ODP site 976	36.20	-4.30	-1108	MARI	8	0	0
ODP1019	41.66	-124.91	989	MARI	8	0	0
ODP1078C	-11.92	13.40	-426	MARI	/	/	/
ODP893A	34.28	-120.03	-577	MARI	8	0	0
Potato Lake	34.45	-111.33	2222	TERR	4	0	0
Rice Lake (Rice Lake 81)	40.30	-123.22	1100	TERR	/	/	/
Siberia	-17.09	-64.72	2920	TERR	2	0	0
Stracciaccappa	42.13	12.32	220	TERR	/	/	/
Tagua Tagua - DIGI	-34.50	-71.16	200	TERR	6	0	0
Taiquemo	-42.17	-73.60	170	TERR	/	/	/
Toushe Basin	23.82	120.88	650	TERR	/	/	/
Tswaing Crater	-25.40	28.08	1100	TERR	/	/	/
Tyrrendara Swamp	-38.20	141.76	13	TERR	/	/	/
Valle di Castiglione	41.90	12.76	44	TERR	/	/	/
W8709-13 PC	42.11	-125.75	-2712	MARI	8	0	0
W8709-8 PC	42.26	-127.68	-3111	MARI	8	1	1



453

Walker Lake	35.38	-111.71	2500	TERR	/	/	/
-------------	-------	---------	------	------	---	---	---

454



455 Table 2. Leave-out cross-validation (with geographically and climatically close sites removed)
 456 using $fxTWA$ -PLSv2 for mean temperature of the coldest month (MTCO), mean temperature
 457 of the warmest month (MTWA) and plant-available water (α) with P-splines smoothed fx
 458 estimation and bins of 0.02, 0.02 and 0.002, respectively. n is the number of components where
 459 the last significant number of components is indicated in **bold**. Avg.bias is the average bias;
 460 RMSEP is the root-mean-square error of prediction; and $\Delta RMSEP$ is the per cent change of
 461 RMSEP, which is $100 \times (RMSEP_n - RMSEP_{n-1})/RMSEP_{n-1}$; when $n = 1$, $RMSEP_0$ is the
 462 RMSEP of the null model. p assesses whether using the current number of components is
 463 significantly different from using one component less. The degree of overall compression is
 464 assessed by linear regression of the cross-validated reconstructions on to the climate
 465 variable; b_1 and $b_1.se$ are the slope and the standard error of the slope, respectively. The closer
 466 the slope (b_1) is to 1, the less the compression.

	n	R^2	Avg.bias	RMSEP	$\Delta RMSEP$	p	b_1	$b_1.se$
MTCO (°C)	1	0.72	-1.11	6.83	-45.45	0.001	0.83	0.00
	2	0.74	-1.21	6.68	-2.25	0.001	0.84	0.00
	3	0.75	-1.10	6.51	-2.48	0.001	0.85	0.00
	4	0.75	-1.10	6.54	0.53	1.000	0.85	0.00
	5	0.75	-1.13	6.54	-0.07	0.188	0.85	0.00
MTWA (°C)	1	0.54	-0.33	3.89	-29.76	0.001	0.66	0.00
	2	0.58	-0.32	3.69	-5.10	0.001	0.71	0.00
	3	0.59	-0.33	3.68	-0.14	0.001	0.71	0.00
	4	0.59	-0.33	3.69	0.07	0.746	0.71	0.00
	5	0.59	-0.33	3.67	-0.39	0.001	0.71	0.00
α	1	0.62	-0.02	0.189	-37.73	0.001	0.66	0.00
	2	0.63	-0.022	0.188	-0.81	0.001	0.68	0.00
	3	0.63	-0.021	0.186	-0.87	0.001	0.68	0.00
	4	0.65	-0.02	0.182	-2.11	0.001	0.71	0.00
	5	0.65	-0.02	0.182	0.11	1.000	0.71	0.00



467 Table 3: Maximum likelihood estimates of the relationship between the change in mean
468 temperature of the coldest month (ΔMTCO) and the change in mean temperature of the
469 warmest month (ΔMTWA) by latitudinal bands for the northern extratropics (NET, north of
470 23.5°N), tropics (TROP, between 23.5°N and 23.5°S) and southern extratropics (SET, south of
471 23.5°S). The intercepts were set to zero since both variables are changes. Coefficients in bold
472 mean both the lower 95% and upper 95% estimates are above 0.

Region		Coefficient	Standard error (SE)	Lower 95%	Upper 95%
NET	Slope	2.129	0.657	0.841	3.417
TROP	Slope	2.276	1.381	-0.431	4.983
SET	Slope	0.979	0.151	0.684	1.275

473

474



475 Table 4: Maximum likelihood estimates of the relationship between the change in plant-
476 available water ($\Delta\alpha$) and the change in mean temperature of the warmest month (ΔMTWA) by
477 latitudinal bands for the northern extratropics (NET, north of 23.5°N), tropics (TROP, between
478 23.5°N and 23.5°S) and southern extratropics (SET, south of 23.5°S). The intercepts were set
479 to zero since both variables are changes. Coefficients in bold mean both the lower 95% and
480 upper 95% estimates are above 0.

Region		Coefficient	Standard error (SE)	Lower 95%	Upper 95%
NET	Slope	0.082	0.022	0.039	0.124
TROP	Slope	0.075	0.026	0.024	0.127
SET	Slope	0.031	0.003	0.025	0.037

481